

Kinetic and Theoretical Study of the Hydrodechlorination
of CH_{4-x}Cl_x (x = 1–4) Compounds on Palladium[†]Nan Chen,^{‡,⊥} Robert M. Rioux,[§] Luis A. M. M. Barbosa,^{||,¶} and Fabio H. Ribeiro^{*‡}

[‡]School of Chemical Engineering, Purdue University, 480 Stadium Mall Drive, West Lafayette, Indiana 47907-2100, [§]Department of Chemical Engineering, The Pennsylvania State University, University Park, Pennsylvania 16802-4400, and ^{||}Schuit Institute of Catalysis, Eindhoven University of Technology, Eindhoven, The Netherlands. [⊥]Current address: Chevron Corporation, 100 Chevron Way, Richmond, California 94802. [¶]Current address: Research and Development, Diagnostic/Delivery System Development and R&D, Covidien Pharmaceuticals, The Netherlands.

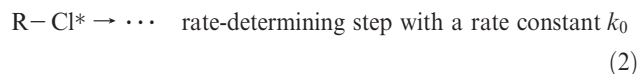
Received May 21, 2010. Revised Manuscript Received July 19, 2010

The reaction kinetics of hydrodechlorination (HDCl) for a series of CH_{4-x}Cl_x (x = 1–4) compounds were measured on a Pd/carbon catalyst. The rate of HDCl correlated with the C–Cl bond energy, suggesting scission of this bond in the molecularly adsorbed molecule is rate-determining. The measured reaction kinetics of the CH_{4-x}Cl_x compounds support a previously proposed Langmuir–Hinshelwood type reaction mechanism. Kinetic and isotope exchange experiments demonstrated the following: gas phase H₂ and HCl are in equilibrium with surface H and Cl; adsorbed Cl is the most abundant surface intermediate; and irreversible scission of the first C–Cl bond is rate-determining. The overall hydrodechlorination reaction rate can be written as $kK_{R-Cl}[R-Cl]/(1+K_{HCl}[HCl]/K_{H_2}^{1/2}[H_2]^{1/2})$. The activation energy of the rate-determining step was related linearly to the dissociation energy of the first C–Cl bond broken in a Brønsted–Evans–Polanyi relationship. This behavior is in agreement with a previous study of CF₃CF_{3-x}Cl_x compounds. During the reaction of CH₃Cl, CH₂Cl₂, and CHCl₃ with deuterium, H–D exchange occurred in only 2%, 6%, and 9% of products, respectively. The increasing H–D exchange with Cl content suggests the steps which determine selectivity in these multipath, parallel reactions. The density functional theory (DFT)-calculated activation energies for the dissociation of the first C–Cl bond in the family of chlorinated methane compounds are in good agreement with the values extracted from kinetic modeling, suggesting that parameters estimated from DFT calculations may be used to estimate the reactivity of a particular chlorinated compound within a family of chlorocarbons.

1. Introduction

Hydrodechlorination (HDCl) is the reaction between H₂ and an organic molecule containing C–Cl bond(s) in which Cl is replaced with hydrogen. Hydrodechlorination is an important step in many syntheses that use a chlorine-containing molecule as an intermediate, for example, in the manufacture of CF₃–CFH₂ (a widely used refrigerant) from CF₃–CFCl₂.¹ The removal of chlorine from a compound requiring disposal can be accomplished by HDCl; this removal may be mandatory before the compounds can be released into the environment due to the adverse effect of chloro-containing molecules on the ozone layer or due to the difficulty to naturally biodegrade these compounds. Applications of hydrodechlorination are in the conversion of unwanted chlorinated compounds into useful ones as, for example, in the conversion of waste 1,2-dichloropropane into propylene² and 1,1,2-trichloroethene into ethane.³ The reaction is

usually performed in the presence of noble metal catalysts; Pd is the most active, selective, and stable catalyst for this reaction,⁴ and recent studies have shown that Pd–Au alloys are active and stable for aqueous-phase hydrodechlorination.^{3,5,6} We previously proposed the rate-determining step consisted of the irreversible scission of the C–Cl bond; equilibrium between gas-phase species (H₂ and HCl) with adsorbed H and Cl.⁷ This proposed rate-determining step was deduced from the reaction kinetic measurements and a correlation between C–Cl bond strength and the overall reaction rate. The reaction steps proposed by Thompson et al.⁷ were supported by recent isotopic tracing experiments.⁸ This set of proposed reaction steps is summarized below in Scheme 1:



$$r = k_0 K_{RCl} [R-Cl^*] [*] \quad \text{rate expression} \quad (3)$$

[†]Part of the Molecular Surface Chemistry and Its Applications special issue.

*To whom correspondence should be addressed. E-mail: fabio@purdue.edu. Telephone: (765) 494-7799. Fax: (765) 494-0805.

(1) Ainbinder, Z.; Manzer, L. E.; Nappa, M. J. In *Handbook of Heterogeneous Catalysis*; Ertl, G., Knozinger, H., Weitkamp, J., Eds.; VCH: Weinheim, 1997; pp 1677–1685.

(2) Harley, A. D.; Holbrook, M. T.; Smith, D. D.; Cisneros, M. D.; Ito, L. N.; Murchison, C. B. *Processes for converting chlorinated byproducts and waste products to useful materials*; U.S. Patent 5453557, 1995.

(3) Heck, K. N.; Nutt, M. O.; Alvarez, P.; Wong, M. S. *J. Catal.* **2009**, *267*, 97–104.

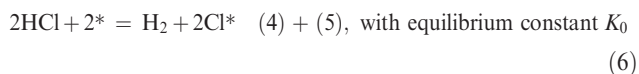
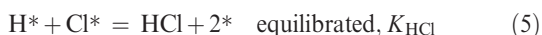
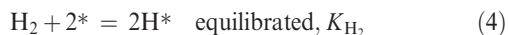
(4) Rayland, R. N. *Catalytic Hydrogenation in Organic Synthesis*; Academic Press: New York, 1979, p 235.

(5) Heck, K. N.; Janesko, B. G.; Scuseria, G. E.; Halas, N. J.; Wong, M. S. *J. Am. Chem. Soc.* **2008**, *130*, 16592–16600.

(6) Wong, M. S.; Alvarez, P. J. J.; Fang, Y. L.; Akcin, N.; Nutt, M. O.; Miller, J. T.; Heck, K. N. *J. Chem. Technol. Biotechnol.* **2009**, *84*, 158–166.

(7) Thompson, C. D.; Rioux, R. M.; Chen, N.; Ribeiro, F. H. *J. Phys. Chem. B* **2000**, *104*, 3067–3077.

(8) Chen, N.; Rioux, R. M.; Ribeiro, F. H. *J. Catal.* **2002**, *211*, 192–197.



The site balance is composed of adsorbed atomic chlorine and vacant sites:

$$[*] + [\text{Cl}^*] = [\text{L}] \quad \text{site balance} \quad (7)$$

and solving for the concentration of free sites

$$[*] = \frac{[\text{L}]}{1 + K_0^{1/2} \frac{[\text{HCl}]}{[\text{H}_2]^{0.5}}} \quad \text{free site concentration} \quad (8)$$

The overall rate can be derived.

$$r = \frac{k'[\text{R}-\text{Cl}]}{1 + K' \frac{[\text{HCl}]}{[\text{H}_2]^{0.5}}} \quad \text{with } k' = k_0 K_{\text{RCl}}[\text{L}] \text{ and } K' = K_0^{1/2} \quad (9)$$

The overall site balance assumes that the surface is covered with atomic chlorine. Chlorine is removed from the surface by reaction with hydrogen to produce HCl. The product HCl inhibits the overall reaction rate (inverse first-order influence on the kinetics).^{7,9}

In many of the molecules we have studied previously^{7–10} and those presented here, multiple chlorine groups can be removed by HDCl. We have determined based on the fact that the selectivity to different products is independent of conversion that removal of chlorine atoms happens while the molecule is adsorbed on the surface, where multiple chlorine atoms can be abstracted. The reactivity of the product molecules is much lower than that of the reactant, and they do not react appreciably. The lower reactivity is caused by the addition of hydrogen in place of chlorine which makes the remaining C–Cl bonds stronger. The hydrodechlorination of chlorofluorocarbons with deuterium demonstrated significant H–D exchange, yielding mechanistic implications for reaction steps beyond the C–Cl bond scission.^{10,11}

In this paper, we extend our work on the kinetics and mechanism of Pd-catalyzed HDCl to the complete series of chlorinated methane compounds, $\text{CH}_{4-x}\text{Cl}_x$. A experimental and theoretical investigation of the kinetics of HDCl for the chlorinated methane compounds is presented. We demonstrate that the hydrodechlorination reaction kinetics of these four compounds can be described by a set of reaction steps previously proposed to describe the kinetics of hydrodechlorination for a series of $\text{CF}_3\text{CF}_x\text{Cl}_{3-x}$ compounds⁷ and shown above. The rates were proportional to the gas-phase bond strength of the C–Cl bond of the chlorinated compounds, similar again to the $\text{CF}_3\text{CF}_x\text{Cl}_{3-x}$ series. The adsorption energy, activation energy, and dissociation energy calculated by density functional theory (DFT) follow the same trend qualitatively as the experimental kinetic results for the $\text{CH}_{4-x}\text{Cl}_x$ compounds. The importance of this work is that the rate of hydrodechlorination for any aliphatic chlorocarbon and chlorofluorocarbon can be

estimated by the calculation of the C–Cl bond strength and the kinetics can be safely assumed to be the same as the one derived here.

2. Experimental Methods

2.1. Catalysts. The 5% Pd catalyst supported on activated carbon used in this study was obtained from Degussa. The catalyst was ground with a mortar and pestle, and the 40/60 mesh fraction was retained for catalytic studies. The characterization of these catalysts has been published previously.^{7,10} The fresh catalyst (200–500 mg) was loaded into the reactor and reduced for 3 h at 300 °C with a hydrogen flow rate of 50 cm³ min^{−1}. The catalysts were treated with the same flow rate of hydrogen for 0.5 h at 150 °C for repeat catalytic experiments.

2.2. Reactants. The chlorinated methane compounds were purchased from Sigma-Aldrich Chemical Co. (CH_3Cl , CCl_4) or Lancaster Synthesis (CH_2Cl_2 , CH_3Cl) and used without further purification. A mixture of 15–20% hydrogen chloride in helium (Matheson) was made with technical grade HCl and He (ultrahigh purity (UHP), 99.999%). Hydrogen (BOC) was passed through a Pd membrane (Matheson hydrogen purifier model 8361) before use. Reaction grade (UHP, 99.999%) helium (BOC) was used as a diluent gas and carrier gas for the gas chromatograph after purification in a gas purifier (HP model 5182-3467). Deuterium (Cambridge Isotope Laboratories, 99.6% D_2 ; 0.4% HD) was purified by the same Pd membrane purifier used for the purification of hydrogen.

2.3. Reactor Configuration. The flow rate of gas through the quartz reactor was controlled with series of mass-flow controllers (Porter Instrument Company, Hatfield, PA) connected to a gas manifold constructed of 1/8" diameter stainless steel tubing. Chloroform, carbon tetrachloride, and methylene chloride are liquids at room temperature, and added to the reaction mixture by passing helium through a saturator maintained at a constant temperature using a recirculating bath (Neslab Instrument Inc. RTE-9, Newington, NH). The mass-flow controllers were calibrated with a bubble flow meter except for the He–HCl mixture, which was determined by varying the composition of a mixture of He/HCl and H_2/CH_4 (a mixture of H_2 and 1003 ppm CH_4 (used as an internal standard)), analyzing the mixture with a flame ionization detector to observe the change in signal of the methane peak.

Reactors were fabricated from quartz with the catalyst held on a fritted quartz disk. The reactor operated in either a continuous (as a continuous stirred tank reactor (CSTR)) or well-mixed batch mode. The inlet and effluent flow rates were $\sim 100 \text{ cm}^3 \text{ min}^{-1}$ during CSTR operation. The inlet gas concentrations were adjusted with mass-flow controllers, and the reaction temperature was controlled by using a Eurotherm model 808 temperature controller. The reaction temperature was measured with a K-type thermocouple (Omega Engineering, Inc., Stamford, CT) inserted into a quartz sheath which extended into the catalyst bed. A bellows pump (Senior Flexonics, MB-21, Bartlett, IL) with a recirculation rate of $\sim 1400 \text{ cm}^3 \text{ min}^{-1}$ provided mixing in the reactor. The high recirculation rates enabled differential reactor operation and minimized heat and transport effects. We tested for the presence of heat- and mass- transfer limitations with the Madon–Boudart test.¹² Previous results⁷ demonstrated heat and mass transfer limitations were absent with a Pd/C catalyst supported on a high-surface area microporous carbon, where transport limitations would be most severe. We concluded the kinetic results presented in this study are not affected by heat- and mass-transfer limitations.

The reaction products were analyzed with a modified gas chromatography (GC-HP 5880A)/mass spectrometry (MS-HP5970A) (GC-MS) system. The column used in the GC instrument was a 5% Krytox 143AC, 60/80 Carboxpack BHT 20' \times 1/8"

(9) Ribeiro, F. H.; Gerken, C. A.; Somorjai, G. A.; Kellner, C. S.; Coulston, G. W.; Manzer, L. E.; Abrams, L. *Catal. Lett.* **1997**, *45*, 149–153.

(10) Rioux, R. M.; Thompson, C. D.; Chen, N.; Ribeiro, F. H. *Catal. Today* **2000**, *62*, 269–278.

(11) Campbell, J. S.; Kemball, C. *Trans. Faraday Soc.* **1961**, *57*, 809–820.

(12) Madon, R. J.; Boudart, M. *Ind. Eng. Chem. Fundam.* **1982**, *21*, 438–447.

(Supelco, Bellefonte, PA). The gas mixture was analyzed by the GC flame ionization detector for quantitative analysis. The gases were sampled into the mass-selective detector through a fused silica polyimide capillary (51 μm I.D., 363 μm O.D., 0.75 m length) after separation in the GC column. After analysis, the HCl in the gas mixture was neutralized in a solution of sodium hydroxide prior to exhaust.

2.4. Data Collection Procedure. The reaction was allowed to stabilize for 0.5–1 h at a particular set of conditions before the initial data point was taken. During the course of the experiments, changes in concentration and temperature were chosen in a random order so that any variation in the system would not introduce systematic error. At the end of each experiment, we repeated the first data point in the series. The agreement between repeat experiments verified there was no significant deactivation of the catalyst during the experiment, except for CCl_4 HDCl.

We determined the kinetic parameters, activation energy,¹³ reaction order in chlorocarbon,¹⁴ hydrogen,¹⁵ and hydrogen chloride,¹⁶ and the rate (at different temperatures), while changing the $[\text{HCl}]/[\text{H}_2]$ ratio for each compound. The reactant conversion was maintained at <5% in order to assume differential reactor operation. The reactivity of the individual compounds varied dramatically, requiring measurements of reaction kinetics at low conversion over a large temperature range. HCl was included in the feed of all reactions in order to maintain its concentration constant through the catalyst bed, since HCl inhibits the hydrodechlorination reaction and limits the conversion. We compared data from the same experiments carried out at identical conditions to calculate experimental errors. The maximum error in reaction orders is 25%, and the error in the apparent activation energies was 5 kJ mol^{-1} . The reproducibility of the turnover rate was $\geq 90\%$.

Deuterium-exchange experiments were conducted in a well-mixed batch reactor.¹⁷ The reactor was evacuated to 10^{-5} Torr with a diffusion pump for a 0.5 h before the introduction of reactants. The temperature of the oven was raised to the target temperature at a rate of 5 K min^{-1} . A sample of the gas mixture was taken from the reactor using a gastight 500 μL syringe (Hamilton Company, Reno, NV) through a septum fitted to a union mounted on a sample port on the batch reactor loop. For each data point, $\sim 150 \mu\text{L}$ of the gas mixture was injected into the GC-MS for analysis.

2.5. Density Functional Theory Calculations. All calculations were performed using Vienna Ab-Initio Simulation Package (VASP) code to perform periodic density functional theory (DFT) calculations using pseudopotentials and a plane wave basis set.^{18,19} The DFT was parametrized in the local-density

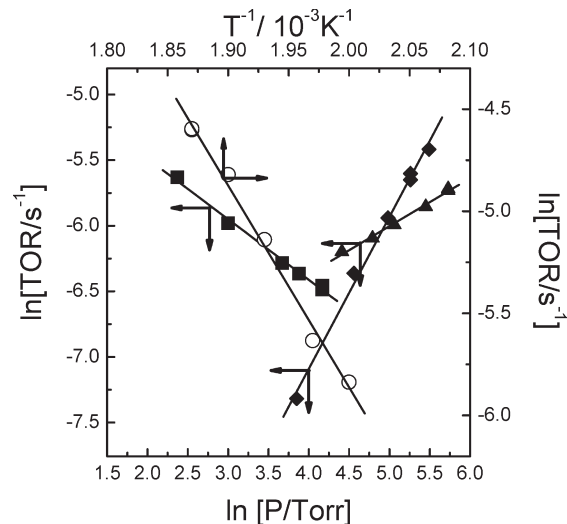


Figure 1. Apparent reaction orders (CH_3Cl (\blacklozenge), H_2 (\blacktriangle), HCl (\blacksquare) and apparent activation energy (\circ) for the hydrodechlorination of CH_3Cl . The reaction conditions are listed below.^{13–17}

approximation (LDA), with the exchange-correlation functional proposed by Perdew and Zunger²⁰ and corrected for nonlocality in the generalized gradient approximations (GGA) using the Perdew–Wang 91 functional.²¹ The interaction between the core and electrons is described using the ultrasoft pseudopotentials introduced by Vanderbilt²² and provided by Kresse and Hafner.²³

The Pd(110) surface is modeled by a periodic five layer-slab with the adsorbate placed on one side of the slab. The unit cell size is 3×3 ; this size enabled the investigation of different adsorbate coverage and the presence of different species simultaneously on the Pd(110) surface. The choice of a limited number of metallic layers in the model is imposed by the size of the system for which a tractable calculation may be performed in reasonable time. One slab is separated from its periodic image in the z -direction by a vacuum space of about 11.4 Å. All atoms, except from the two bottom layers of the slab, were allowed to relax in all optimizations. The value for the bulk Pd–Pd distance was set at 2.81 Å based on the model of Filhol et al.²⁴ in order to reduce the effect of the stress in the metallic layer. This optimized value is in good agreement with the experimentally determined Pd–Pd bulk distance of 2.75 Å.²⁵

In all calculations performed here, the Brillouin-zone integrations have been done on a $2 \times 3 \times 1$ Monkhorst-Pack grid of k -points for all structures, which yields a correct convergence for the calculated energy (at a reasonable computational cost). The search for the transition state is done by following the reaction coordinate and further optimization of the stationary point along this reaction path, as described elsewhere.²⁶ These transition states were further checked by frequency calculations using a VASP internal routine. The surface was kept frozen during these calculations. In most of the cases, only one imaginary frequency was found. In the few cases where two imaginary frequencies were found, the second one was negligible, as observed previously in a study of chlorinated molecules.²⁶

Gas phase C–Cl bond strength values for $\text{CH}_{4-x}\text{Cl}_x$ ($x = 1–4$) were calculated by ab initio DFT calculations using the commercially available Gaussian 98 software package, with the B3PW91/6-311+G(2d,p)//B3PW91/6-311+G(2d,p) functional and basis set. For each compound, the energy of the chlorocarbon, energy of

(13) The conditions for the determination of the apparent activation energy for the four chlorinated methane compounds were as follows: 48–92 °C, 10 Torr CCl_4 , 155 Torr H_2 , and 58 Torr HCl (CCl_4); 92–143 °C, 14 Torr CHCl_3 , 235 Torr H_2 , and 48 Torr HCl (CHCl_3); 187–229 °C, 22 Torr CH_2Cl_2 , 196 Torr H_2 , and 38 Torr HCl (CH_2Cl_2); 227–261 °C, 220 Torr CH_3Cl , 181 Torr H_2 , and 74 Torr HCl (CH_3Cl).

(14) The conditions for the determination of the apparent reaction order in chlorinated methane were as follows: 61 °C, 9–16 Torr CCl_4 , 173 Torr H_2 , and 45 Torr HCl (CCl_4); 114 °C, 15–40 Torr CHCl_3 , 237 Torr H_2 , and 49 Torr HCl (CHCl_3); 201 °C, 21–43 Torr CH_2Cl_2 , 199 Torr H_2 , and 38 Torr HCl (CH_2Cl_2); 227 °C, 46–193 Torr CH_3Cl , 159 Torr H_2 , and 64 Torr HCl (CH_3Cl).

(15) The conditions for the determination of the apparent reaction order in hydrogen were as follows: 114 °C, 16 Torr CCl_4 , 129–256 Torr H_2 , and 50 Torr HCl (CCl_4); 114 °C, 18 Torr CHCl_3 , 183–399 Torr H_2 , and 48 Torr HCl (CHCl_3); 198 °C, 25 Torr CH_2Cl_2 , 108–379 Torr H_2 , and 37 Torr HCl (CH_2Cl_2); 224 °C, 145 Torr CH_3Cl , 82–306 Torr H_2 , and 48 Torr HCl (CH_3Cl).

(16) The conditions for the determination of the apparent reaction order in hydrogen chloride were as follows: 115 °C, 17 Torr CCl_4 , 173 Torr H_2 , 17–50 Torr HCl (CCl_4); 115 °C, 20 Torr CHCl_3 , 155 Torr H_2 , 20–64 Torr HCl (CHCl_3); 199 °C, 25 Torr CH_2Cl_2 , 127 Torr H_2 , 22–64 Torr HCl (CH_2Cl_2); 227 °C, 193 Torr CH_3Cl , 159 Torr H_2 , 10–64 Torr HCl (CH_3Cl).

(17) The reaction conditions for the hydrodechlorination of $\text{CH}_{4-x}\text{Cl}_x$ ($x = 1–3$) compounds with deuterium were as follows: 205 °C, 416 Torr CH_3Cl , 434 Torr D_2 (CH_3Cl); 184 °C, 30 Torr CH_2Cl_2 , 261 Torr D_2 (CH_2Cl_2); 95 °C, 18 Torr CH_2Cl_2 , 328 Torr D_2 (CHCl_3).

(18) Kresse, G.; Furthmüller, J. *Phys. Rev. B* **1996**, *54*, 11169–11186.

(19) Kresse, G.; Furthmüller, J. *Comput. Mater. Sci.* **1996**, *6*, 15–50.

(20) Perdew, J. P.; Zunger, A. *Phys. Rev. B* **1981**, *23*, 5048–5079.

(21) Perdew, J. P.; Yue, W. *Phys. Rev. B* **1986**, *33*, 8800–8802.

(22) Vanderbilt, D. *Phys. Rev. B* **1990**, *41*, 7892–7895.

(23) Kresse, G.; Hafner, J. *J. Phys.: Condens. Matter* **1994**, *6*, 8245–8257.

(24) Filhol, J. S.; Simon, D.; Sautet, P. *J. Phys. Chem. B* **2003**, *107*, 1604–1615.

(25) Kittel, C. *Introduction to Solid State Physics*; John Wiley: Chichester, 1996.

(26) Barbosa, L. A. M. M.; Sautet, P. *J. Catal.* **2002**, *207*, 127–138.

Table 1. Kinetic Data for the Hydrodechlorination of Chlorinated Hydrocarbons on Pd/C

reactant	reaction temperature (°C)	products	TOR (s ⁻¹) ^a (selectivity) ^b	E _{a,app} (kJ mol ⁻¹)	reaction order		
					chlorinated hydrocarbon	H ₂	HCl
CH ₃ Cl	227	CH ₄	(7.27 ± 0.21) × 10 ⁻⁵ (100)	82 ± 4	1.16 ± 0.04	0.37 ± 0.02	-0.46 ± 0.02
CH ₂ Cl ₂	201	CH ₄	(1.07 ± 0.01) × 10 ⁻² (62)	93 ± 5	1.04 ± 0.12	0.44 ± 0.02	-0.61 ± 0.04
		CH ₃ Cl	(7.25 ± 0.35) × 10 ⁻³ (38)	80 ± 3	1.08 ± 0.16	0.68 ± 0.06	-0.60 ± 0.03
CHCl ₃	114	CH ₄	(2.09 ± 0.11) × 10 ⁻¹ (82)	86 ± 5	0.44 ± 0.02	0.81 ± 0.02	-0.54 ± 0.03
		CH ₃ Cl	(1.02 ± 0.04) × 10 ⁻² (4)	76 ± 2	0.26 ± 0.03	0.65 ± 0.05	-0.32 ± 0.03
		CH ₂ Cl ₂	(3.41 ± 0.38) × 10 ⁻² (14)	90 ± 7	0.7 ± 0.05	0.26 ± 0.06	-0.61 ± 0.04
CCl ₄ ^c	61	CH ₄	(3.27 ± 0.25) × 10 ⁻¹ (30)	62 ± 3	0.26 ± 0.04	0.55 ± 0.02	-0.45 ± 0.03
		CH ₃ Cl	(1.77 ± 0.11) × 10 ⁻¹ (15)	64 ± 4	0.78 ± 0.05	0.32 ± 0.04	-0.60 ± 0.06
		CH ₂ Cl ₂	(6.77 ± 0.36) × 10 ⁻² (6)	52 ± 4	0.48 ± 0.06	0.25 ± 0.05	-0.43 ± 0.04
		CHCl ₃	(5.38 ± 0.26) × 10 ⁻¹ (49)	54 ± 3	0.33 ± 0.08	0.16 ± 0.03	-0.34 ± 0.06
CF ₃ -CFHCl ^d	223	CF ₃ -CH ₂ F	1.6 × 10 ⁻⁴ (99.9)	95	1.1	0.4	-0.8
		CF ₃ -CH ₃	2.0 × 10 ⁻⁷ (0.1)	80	1.0	0.3	-0.3

^a Turnover rates corrected for 150 Torr chlorinated reactant, 200 Torr H₂, 20 Torr HCl, and 150 °C. ^b The selectivity was independent of conversion. ^c Hydrocarbon byproducts were also detected (only initially): C₂H₄/C₂H₆, C₃H₆/C₃H₈, C₄H₈/C₄H₁₀, and C₅H₁₀/C₅H₁₂. ^d Reproduced from ref 7.

radical R• formed by loss of the first Cl, and energy of Cl• radical were calculated. The C–Cl bond dissociation energy was defined as the energy difference, $E(\text{R}-\text{Cl}) = E(\text{R}\cdot) + E(\text{Cl}\cdot) - E(\text{RCl})$.

3. Results

3.1. Hydrodechlorination Reaction Kinetics of CH_{4-x}-Cl_x (x = 1–4). An example of the kinetic data collected is shown in Figure 1 for CH₃Cl. Table 1 summarizes the hydrodechlorination reaction kinetics, including apparent activation energy, apparent reaction orders, reaction rate, and selectivity for a series of CH_{4-x}-Cl_x (x = 1–4) compounds and CF₃-CHFCl on a Pd/C catalyst. The temperature at which the kinetic measurements were conducted to maintain differential conditions is given in Table 1. Rates were corrected to the standard condition of 150 Torr chlorinated reactant, 200 Torr H₂, 20 Torr HCl, and 150 °C using the measured reaction orders to account for partial pressure differences and activation energy to correct for temperature differences. Reaction rates for the four chlorinated methanes decrease in the order CH₃Cl < CH₂Cl₂ < CHCl₃ < CCl₄, demonstrating that the rate of hydrodechlorination increased with the number of chlorine atoms in the molecule. A similar trend was observed for a series of CF₃CF_{3-x}-Cl_x (x = 1–3) compounds.⁷ With the exception of CCl₄, no significant deactivation occurred during the course of reaction.

With the exception of CH₃Cl, C₁ products containing up to three chlorines were detected. The selectivity toward these products was independent of conversion over the conversion range explored in this study. The conversion of CH₂Cl₂ varied from 2 to 25%, while the selectivity to methane (62%) and CH₃Cl (38%) remained constant. The selectivity was constant during the hydrodechlorination of CHCl₃ over a conversion range of 2–21%; similarly, the selectivity was constant during the hydrodechlorination of CCl₄ over a conversion range of 5–15% (see Table 1). During the hydrodechlorination of CCl₄, hydrocarbons such as C₂H₄, C₂H₆, C₃H₆, C₃H₈, C₄H₈, C₄H₁₀, C₅H₁₀, and C₅H₁₂ were detected in addition to methane and the chlorinated methane products. The selectivity to byproduct was time dependent. From a test performed at 60 °C while holding all gas concentrations constant, the CCl₄ total conversion was 37% initially with 29% transformed to byproduct and only 8% to CH₄, CH₂Cl₂, and CHCl₃. As the catalyst deactivated, the byproduct formation decreased. After about 160 min time on stream, the byproduct formation fell below the detection limit and conversion toward hydrodechlorination compounds stabilized at 7%.

For comparison, the rate, selectivity, and kinetic parameters of CF₃CFHCl HDCl are included in Table 1. The apparent HCl

reaction order for the chlorinated methanes was less negative than the apparent HCl order for CF₃CFHCl. The HCl order varied from -0.9 to -0.8 for CF₃CFHCl and from -0.6 to -0.5 for CH₃Cl with temperature (213–244 °C). The reaction order of CHCl₃ increased from 0.1 to 0.5 as the temperature decreased from 135 to 100 °C. This behavior differs from Langmuir-type adsorption. The overall lower reaction order in CHCl₃ is attributed to condensation of CHCl₃ in the micropores of the carbon support.⁷

3.2. Determination of *k'* and *K'* from Langmuir–Hinshelwood Rate Expression. The two constants, *k'* and *K'*, in eq 9 can be extracted from the hydrodechlorination kinetics. The linear form of the rate expression (eq 9) is

$$\frac{1}{r} = \frac{1}{k'[\text{R}-\text{Cl}]} + \frac{K'}{k'[\text{R}-\text{Cl}]} \times \frac{[\text{HCl}]}{[\text{H}_2]^{0.5}} \quad (10)$$

Equation 10 demonstrates that at a plot of 1/*r* (inverse of the TOR at a constant R–Cl partial pressure) as a function of the partial pressure ratio, [HCl]/[H₂]^{1/2}, can be used to determine the lumped rate constant, *k'*, and the equilibrium constant, *K'*, for the reaction between adsorbed H and Cl to form HCl. Figure 2 shows the results from a HCl reaction order experiment for CH₃Cl HDCl plotted according to eq 10, with the values of the best fit line shown in the figure. We predicted the HDCl reaction rate of a given chlorinated compound using eq 9 after the determination of *k'* and *K'*.

The rate and equilibrium constants were determined at four different temperatures which allowed us to determine the temperature dependence of *k'* and *K'* (as explained in section 3.3). A nonlinear parameter estimation was conducted by varying the pre-exponential factors on *k'* and *K'* to all 44 data points taken for each compound. The predicted rate versus measured rate for CH₃Cl at 227 °C is shown in Figure 3.

3.3. Temperature Dependence for *k'* and *K'*. The temperature dependence of the lumped rate and equilibrium constants, *k'* and *K'*, was determined for the series of CH_{4-x}-Cl_x compounds and CF₃CFHCl²⁷ in Figures 4 and 5, respectively. The rate constant, *k'*, is the product of two terms, the equilibrium constant of adsorption of the chlorinated organic compound and the kinetic rate constant for the proposed rate-determining step (eq 2).

(27) The reaction conditions for the determination of the temperature dependence of the hydrogen chloride reaction order were as follows: 41, 51, 70, and 115 °C, 17 Torr CCl₄, 173 Torr H₂, 17–50 Torr HCl (CCl₄); 91, 100, 115, and 124 °C, 20 Torr CHCl₃, 155 Torr H₂, 20–64 Torr HCl (CHCl₃); 188, 199, 210, and 220 °C, 25 Torr CH₂Cl₂, 127 Torr H₂, 22–64 Torr HCl (CH₂Cl₂); 213, 227, 237, and 244 °C, 193 Torr CH₃Cl, 159 Torr H₂, 10–64 Torr HCl (CH₃Cl); 216, 226, 236, and 247 °C, 132 Torr CF₃CFHCl, 211 Torr H₂, 11–41 Torr HCl (CF₃CFHCl).

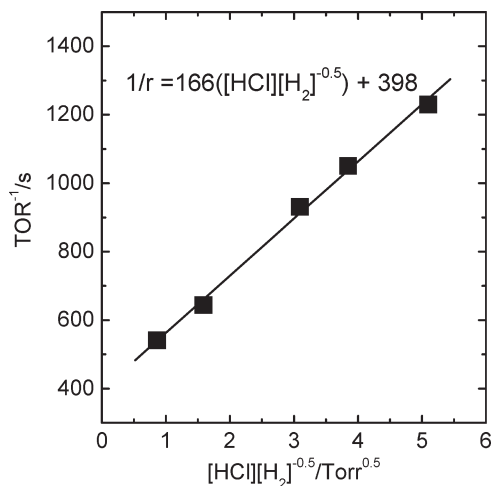


Figure 2. Calculation of k' and K' from the turnover rate (TOR) data for CH_3Cl obtained from the measurement of the HCl reaction order (i.e., the ratio of $[\text{HCl}]/[\text{H}_2]^{0.5}$ was changed by increasing $[\text{HCl}]$). The linear form of the rate equation (eq 10) is provided; the slope is equal to $K'/k'[\text{R}-\text{Cl}]$, and the intercept is equal to $1/k'[\text{R}-\text{Cl}]$. The reaction conditions were 193 Torr CH_3Cl , 211 Torr H_2 , 11–41 HCl, and 226 °C.

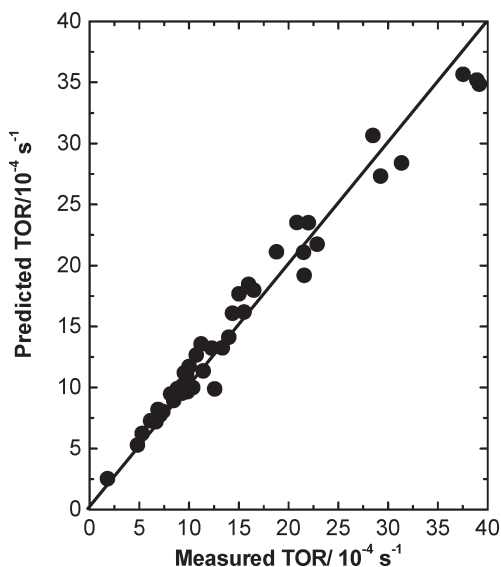


Figure 3. Parity plot of the measured CH_3Cl hydrodechlorination reaction rate (solid circles) and predicted rate using eq 9 (solid line) for CH_3Cl .

Therefore, the apparent activation energy is the sum of the heat of adsorption of the $\text{CH}_{4-x}\text{Cl}_x$ and the activation energy for the rate-determining step. Unfortunately, the current kinetic model does not allow the determination of the true activation energy because there is no independent measure of $K_{\text{R-Cl}}$ (or $\Delta H_{\text{ads,R-Cl}}$). The heat of adsorption of $\text{R}-\text{Cl}$ determined from DFT calculations (see section 3.6, Table 3) ranged from 35 to 47 kJ mol^{-1} .

The term K' was used to evaluate the heat of the overall HCl formation reaction (eq 6). This lumped constant is the ratio of the equilibrium constant for eq 5 and the square root of the equilibrium constant for eq 4, that is, $K_0 = K_{\text{HCl}}/K_{\text{H}_2}^{1/2}$. Therefore, this constant represents the surface reaction between H^* and Cl^* and the dissociative adsorption of hydrogen (eq 4). Figure 5 demonstrates that the lumped heat of reaction for reaction (6) is negative and differs for each chlorocarbon. In theory, they should be the same since this equilibrium constant is independent of the chlorocarbon.

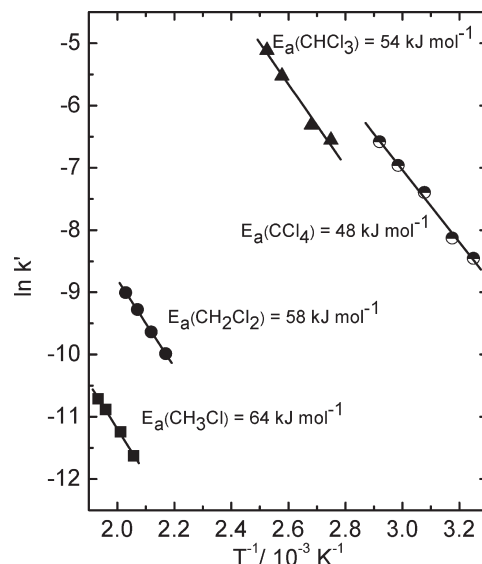


Figure 4. Temperature-dependent behavior of k' from eq 9 for the four $\text{CH}_{4-x}\text{Cl}_x$ ($x = 1-4$) compounds. The constant, k' , is an apparent parameter, a product of the true kinetic rate constant, k_0 , and equilibrium adsorption constant, K_{RCl} .

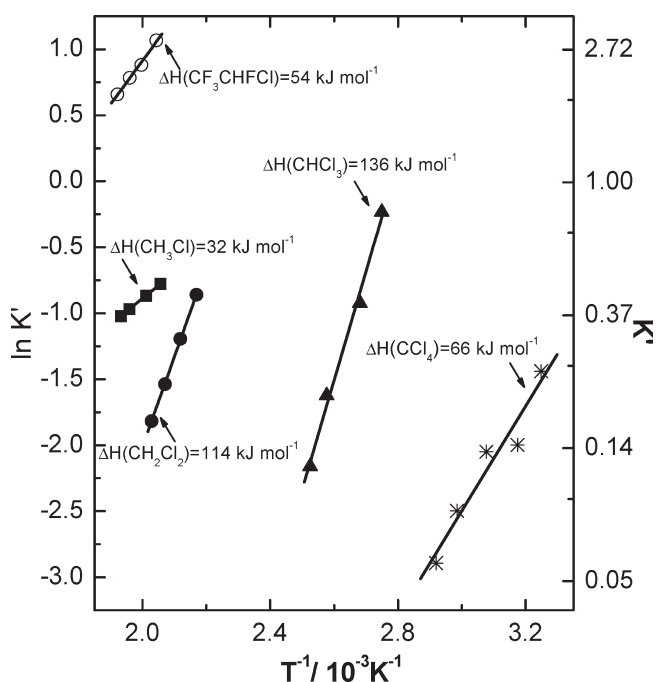


Figure 5. Heat of reaction for the equilibrium between gas phase H_2 , HCl , and surface H , Cl ($2\text{HCl} + 2^* = \text{H}_2 + 2\text{Cl}^*$) for $\text{CH}_{4-x}\text{Cl}_x$ ($x = 1-4$) compounds and CF_3-CFHCl . The equilibrium constant for this reaction, K_0 , is a lumped constant and defined as $K_{\text{HCl}}/K_{\text{H}_2}^{1/2}$ (see Scheme 1 for explanation of constants).

However, the surface coverage varies considerably over the wide temperature range required to maintain differential reactor operation. For example, the difference in reaction temperature at which the kinetics were measured for CH_3Cl and CCl_4 HDCI was 165 °C. This should have a significant influence on the surface coverage and subsequently on the surface energetics.

3.4. C–Cl Bond Energy Calculation and Prediction of Relative Hydrodechlorination Reaction Rates of Chlorinated Methane Compounds. In a previous publication,⁷ we found a correlation between the relative turnover rate of $\text{CF}_3\text{CF}_{3-x}\text{Cl}_x$ ($x = 1-3$)

Table 2. C–Cl Bond Strength of CH_{4-x}Cl_x (x = 1–4) Compounds, Comparison between Measured Turnover Rate and Predicted Rate Using eq 11

compound	C–Cl bond energy (kJ mol ⁻¹) ^a	overall turnover rate (s ⁻¹) ^b	relative turnover rate	predicted relative turnover rate
CH ₃ Cl	346	(7.27 ± 0.21) × 10 ⁻⁵	1	1
CH ₂ Cl ₂	319	(1.79 ± 0.04) × 10 ⁻²	2.46 × 10 ²	1.2 × 10 ²
CHCl ₃	288	0.26 ± 0.01	3.58 × 10 ³	3.3 × 10 ³
CCl ₄	250	1.11 ± 0.05	1.55 × 10 ⁴	8.5 × 10 ⁵

^a Values calculated using Gaussian 98 program; the method used is B3PW91/6-311+G(2d,p)//B3PW91/6-311+G(2d,p). ^b Turnover rates corrected for 150 Torr chlorinated methane, 200 Torr H₂, 20 Torr HCl, and 150 °C.

Table 3. Calculated Energies (in kJ mol⁻¹) for the CH_{4-x}Cl_x Family on the Pd(110) Surface at θ = 1/9 ML

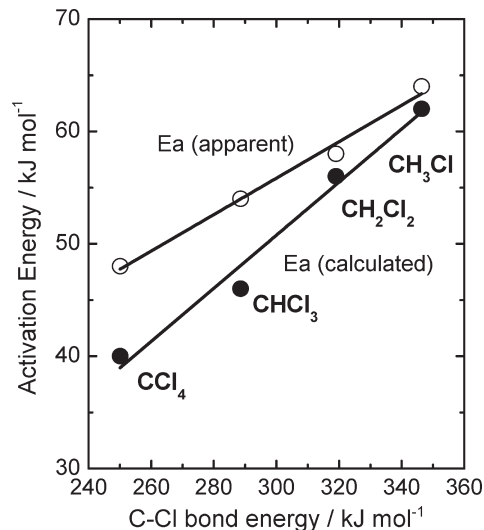
Compound	Adsorption	Dissociation	Activation Energy
CH ₃ Cl	-35	-68	62
CH ₂ Cl ₂	-40	-80	56
CHCl ₃	-44	-128	46
CCl ₄	-47	-159	40

compounds and the bond energy of the first C–Cl bond to be broken. We investigated whether the turnover rate correlated with the gas-phase C–Cl bond strength for the CH_{4-x}Cl_x (x = 1–4) compounds. The gas-phase C–Cl bond energy²⁸ of these chlorinated methane compounds was calculated using Gaussian 98.²⁹ We estimated the relative hydrodechlorination turnover rates of CH_{4-x}Cl_x (x = 1–4) using a method described in a previous publication.⁷ This method is based on the Brønsted–Evans–Polanyi (BEP) relationship,³⁰ which states that, for a family of similar compounds, the difference in activation energy is linearly related to the difference in overall reaction enthalpy. It is used to correlate ΔH_{R-Cl,surface} for C–Cl bond scission of the adsorbed species to the gas-phase C–Cl bond strength, ΔH_{R-Cl, gas}. After this treatment, the ratio of the rate constant of the different chlorinated methane compounds can be expressed as a function of the difference of their gas phase C–Cl bond energy. The detailed derivation of this equation is shown in ref 7.

$$\frac{k_1}{k_2} = e^{-\Delta E_a/RT} = e^{-\alpha(1-\beta)\Delta|\Delta H_{R-Cl}|/RT} \quad (11)$$

This equation allows the calculation of the relative turnover rate for any member in a series of compounds as a function of the turnover rate of an arbitrary reference from the difference in ΔH_{R-Cl} between the reference member (CH₃Cl) and another member of the series (ΔΔH_{R-Cl}). In eq 11, α is a constant from the Polanyi relationship and β is a constant from the linear free energy treatment. A value of 0.5 for the lumped parameter, α(1 – β), yielded the best fit to the experimental data. The values of calculated C–Cl bond energy and relative hydrodechlorination rates are summarized in Table 2. The agreement between predicted relative hydrodechlorination rates and experimental relative rates are within 20%, except for CCl₄. A linear relationship between the measured apparent E_a and calculated E_a of the CH_{4-x}Cl_x (x = 1–4) compounds and their calculated CFC gas-phase C–Cl bond strength is shown in Figure 6.

3.5. Hydrodechlorination in the Presence of Deuterium: Product Distribution and H–D Exchange for a Series of Chlorinated Methane Compounds. The hydrodechlorination reaction in D₂ of the hydrogen-containing chlorinated methane compounds, CH₃Cl, CH₂Cl₂ and CHCl₃, was used to determine which C–H bonds break during reaction. The reaction of CH₃Cl

**Figure 6.** Polyani-type relationship between the gas phase C–Cl bond strength and the activation energy extracted from *k'* (Figure 4) (○) and DFT-calculated activation energy (●) for the CH_{4-x}Cl_x (x = 1–4) compounds.

with D₂ produced CH₃D (96%) and CH₂D₂ (4%). Figure 7A is the product distribution for CH₂Cl₂ in the presence of deuterium; the dominant species formed during the first C–Cl bond scission was the singly deuterated chloromethane, CH₂DCI (94%), and only 6% of the chloromethane (CD₃Cl and CHD₂Cl) contained more than one deuterium. However, for methane, formed by the removal of both chlorines, nearly 35% contained more than two deuterium atoms. A similar trend of increased H–D exchange with increasing degree of Cl removal was also observed during the hydrodechlorination of CHCl₃ with D₂ (Figure 7B). The presence of neighboring C–Cl bond seems to facilitate H–D exchange. The products formed by the *first* C–Cl bond scission and deuteration: for CH₃Cl, there was only 4% multiple deuterated methane; while for CH₂Cl₂, 6% of the chloromethane was enriched with more than one deuterium (CD₃Cl and CHD₂Cl); and for the dichloromethane formed from CHCl₃, the level of multideuteration increased to 8%.

3.6. Periodic DFT Calculations of the Scission of the First C–Cl Bond in Adsorbed Chlorinated Methane Compounds. We have investigated the different adsorption modes for the family of CH_{4-x}Cl_x molecules on the Pd(110) surface. These adsorption modes differ from each other regarding the manner the molecule orients with respect to the Pd(110) surface and its interaction with this surface. The CH_{4-x}Cl_x molecule can approach the surface via its hydrogen and chlorine atom, or via both hydrogen/chlorine and chlorine/chlorine atoms. These different ways of approaching the surface have been investigated here for the family of CH_{4-x}Cl_x molecules on the Pd(110) surface. The most favored interaction of the chlorocarbon molecules with the Pd surface is the simultaneous interaction of more than one atom, with preference for the chlorine atoms. The possible adsorption

(28) The bond energy was determined by taking the difference in energy of the molecule and its fragments: $E(A - B) = E(A) + E(B) - E(AB)$.

(29) Foresman, J. B.; Frish, A. *Exploring Chemistry with Electronic Structure Methods*; Gaussian Inc.: Pittsburgh, PA, 1996.

(30) Boudart, M.; Djega-Mariadassou, G.; *Kinetics of Heterogeneous Catalytic Reactions*; Princeton University Press: Princeton, NJ, 1984; p 222.

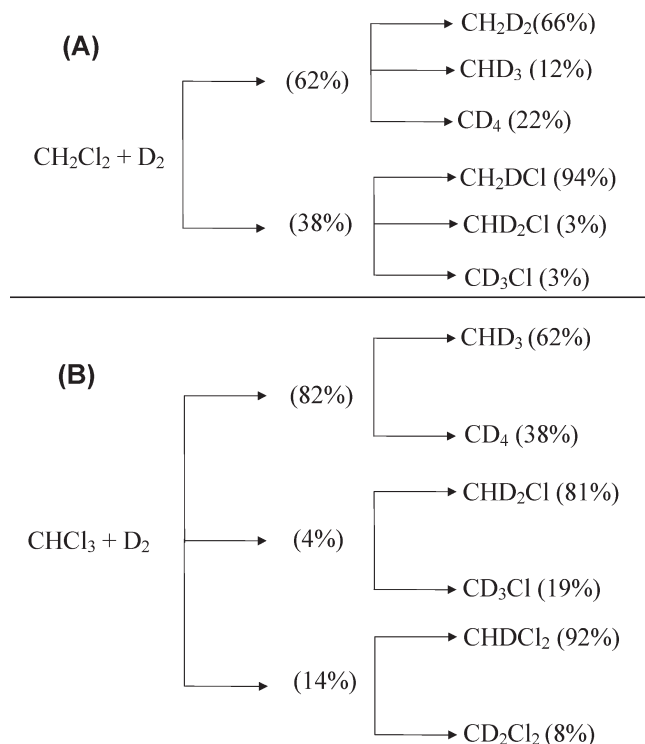


Figure 7. (A) Product distribution for the hydrodechlorination of CH_2Cl_2 with deuterium. The reaction conditions were 30 Torr CH_2Cl_2 , 200 Torr D_2 , and balance He. The batch reactor conversion varied from 7 to 21% with reaction temperatures between 184 and 235 °C. (B) Product distribution for the hydrodechlorination of CHCl_3 with deuterium. The reaction conditions were 18 Torr CHCl_3 , 328 Torr D_2 , and balance He. The batch reactor conversion varied from 6 to 23% with reaction temperatures between 95 and 135 °C. The selectivity was independent of conversion.

modes on the (110) surface are top, shortbridge, longbridge and hollow. The most stable adsorption site is the top adsorption mode. There are two possible orientations for the top adsorption mode: one is along the $[-110]$ direction (referred to as top/shortbridge) and another is along the $[001]$ direction (referred to as top/long-bridge). The energy difference between these configurations is very small, only 4 kJ mol^{-1} . This small energy difference between the top/short-bridge and top/long-bridge orientations is similar for all members of the $\text{CH}_x\text{Cl}_{4-x}$ family. The top adsorption modes are presented in Figure 8 for the case of CH_3Cl .

For the case of CHCl_3 and CCl_4 , three Cl atoms interact with the Pd surface, two at a top adsorption site, regardless of the orientation on the Pd surface (long- or short-bridge). This adsorption mode is the most favorable interaction with the surface for these two molecules because of their tetrahedral configuration. In Figure 9, the top/long-bridge orientations of CHCl_3 and CCl_4 are presented. While the two top orientations have very similar adsorption energy, the dissociation energy of the first C–Cl bond differs significantly. For bulky members of the $\text{CH}_x\text{Cl}_{4-x}$ family, such as CHCl_3 and CCl_4 , the dissociation of the first C–Cl bond is hampered by steric effects of the chlorine atoms. Figure 10 demonstrates the influence of steric effects with added chlorine atoms using CH_2Cl_2 and CCl_4 as examples. The dissociated chlorine atom cannot access the favored short-bridge adsorption site on the metallic row for the case of CCl_4 , while the dissociated chlorine atom can easily be accommodated at the favored short-bridge position for the smaller member of the $\text{CH}_x\text{Cl}_{4-x}$ family (see CH_2Cl_2 in Figure 10b). As a consequence of this steric hindrance, the value for the dissociation energy found

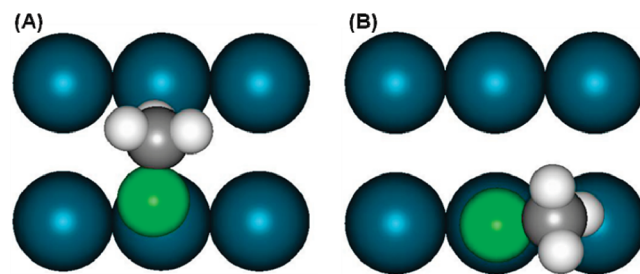


Figure 8. The most stable configurations of CH_3Cl at $\theta = 1/9 \text{ ML}$ on the Pd(110) surface. (A) Top-down view of both H and Cl adsorbed at a top/long-bridge orientation and (B) top-down view of H and Cl adsorbed at a top/shortbridge orientation.

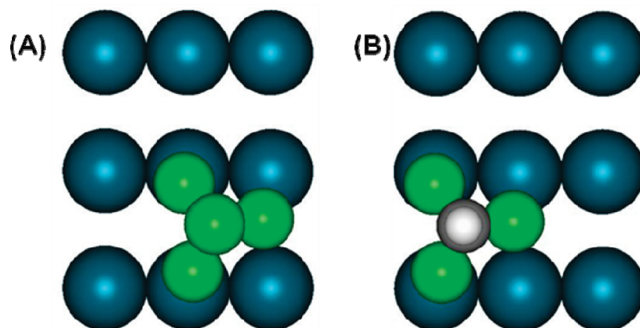


Figure 9. The most stable adsorption configuration of (A) CCl_4 and (B) CHCl_3 at $\theta = 1/9 \text{ ML}$ on the Pd(110) surface with both H and Cl adsorbed in a top/long-bridge orientation.

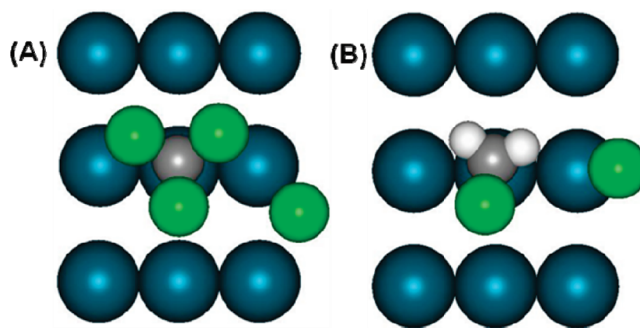


Figure 10. The most stable configuration of (A) CCl_4 and (B) CH_2Cl_2 dissociation products at $\theta = 1/9 \text{ ML}$ on the Pd(110) surface starting from the top adsorption mode with both H and Cl possessing a top/short-bridge orientation.

for the top/short-bridge orientation is 20 kJ mol^{-1} smaller than the top/long-bridge orientation for the two bulkiest molecules (CHCl_3 and CCl_4). The steric effect between the two dissociated fragments does not occur at the top/long-bridge orientation because of the greater distance between two Pd atoms in the $[001]$ direction on the Pd(110) surface. Due to the difficulty associated with dissociation along the $[-110]$ direction on the Pd(110) surface, all energies found in Table 3 for each member of the $\text{CH}_x\text{Cl}_{4-x}$ family are related to the top adsorption site along the $[001]$ direction of the Pd(110) surface (top/long-bridge orientation).

In Table 3, the adsorption energy, the dissociation energy of the first C–Cl bond, and the respective activation energy for dissociation of the first C–Cl bond for each member of the $\text{CH}_x\text{Cl}_{4-x}$ family are presented. The adsorption energy increases with the number of chlorine atoms in the parent molecule. Starting with the monochloromethane, each new chlorine atom

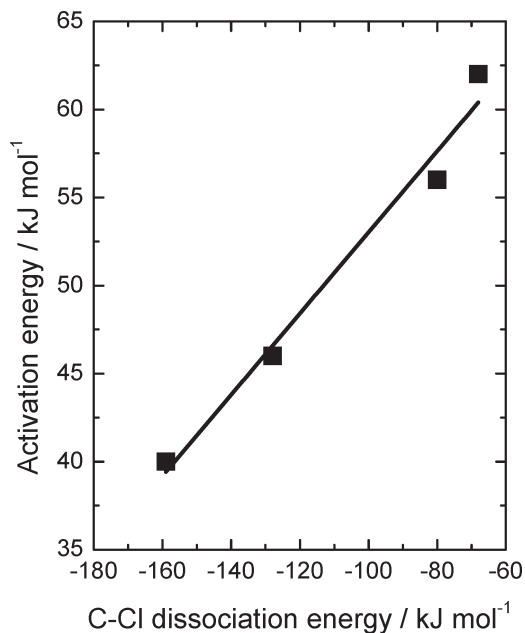


Figure 11. BEP relationship between the activation energy for scission of the first C–Cl bond versus the respective dissociation energy.

adds an average of 4 kJ mol^{-1} per additional chlorine. The dissociation energy also increases, becoming more exothermic as the number of chlorines within the molecule increases from 1 to 4. This may indicate that the $\text{CH}_x\text{Cl}_{3-x}$ fragment interacts more strongly with the Pd surface, when $x \geq 2$. One may expect this result because the chlorine atom is highly electronegative, which makes the $\text{CH}_x\text{Cl}_{3-x}$ fragment electron-withdrawing. The activation energy for the first C–Cl bond scission decreases when more chlorine atoms are present in the original molecule. This is a well-known result, which has been already observed both experimentally and theoretically.^{26,31–33} If one plots the dissociation energy of the first C–Cl bond versus the respective activation energy for the $\text{CH}_x\text{Cl}_{4-x}$ family, a BEP relationship is found (Figure 11). A similar trend was observed between the DFT-calculated activation energy and the gas-phase C–Cl bond strength in the $\text{CH}_{4-x}\text{Cl}_x$ series (Figure 6).

There is a clear distinction between the geometry of the transition state formed during the dissociation of the first C–Cl bond for the members of $\text{CH}_x\text{Cl}_{4-x}$ family. Figure 12 demonstrates the transition states for CH_2Cl_2 and CCl_4 . In the case of CCl_4 , the transition state structure is closer to the initial state (the molecular adsorption configuration) while the transition state for CH_2Cl_2 resembles the final state. This confirms the low activation energy calculated for the dissociation of the first C–Cl bond in CCl_4 . The configuration of the transition state is dependent upon the value of x within the $\text{CH}_{4-x}\text{Cl}_x$ family. For instance, the CCl_3 fragment appears unstable if positioned between Pd atoms along the [001] direction. However, in the case of CH_2Cl_2 , the CH_2Cl fragment is stable along this same direction. This is supported by the shortest distance between the carbon atom from the $\text{CH}_x\text{Cl}_{3-x}$ fragment of the transition state configuration and the Pd surface (found between the fragment and the Pd atom labeled “1”) which is 3.91 and 2.32 Å for CCl_4 and CH_2Cl_2 , respectively. For CH_2Cl_2 , each fragment moves in the opposite direction after C–Cl

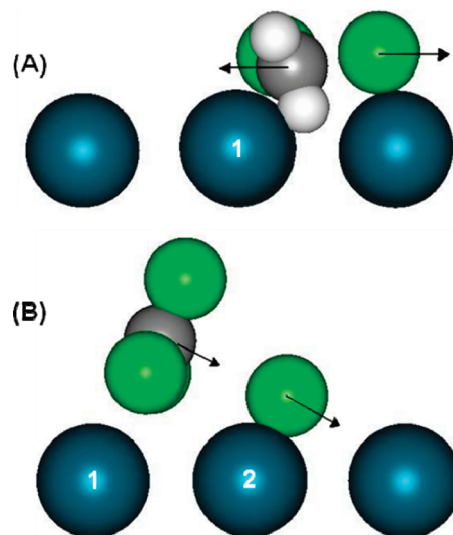


Figure 12. Transition state geometry for (A) CH_2Cl_2 and (B) CCl_4 on Pd(110). The arrows indicate the movement of the individual fragments after dissociation of the first C–Cl bond.

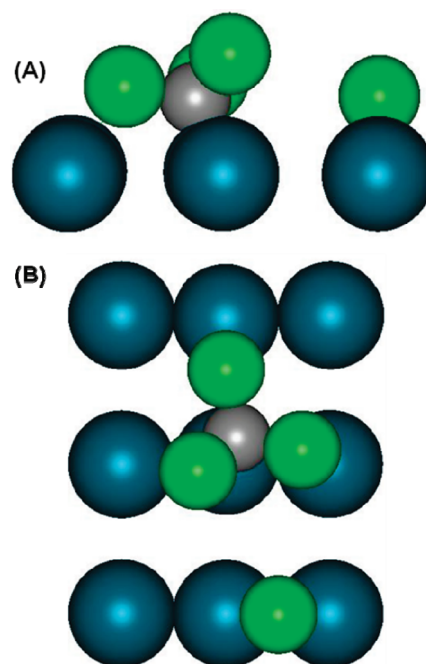


Figure 13. Dissociation of CCl_4 on the Pd(110) surface at $\theta = 1/9 \text{ ML}$. (A) Side view and (B) top-down view.

bond scission. Conversely, the CCl_4 fragments move in the same direction (toward the Pd atom labeled with a “2”), although both CH_2Cl and CCl_3 fragments still interact with the Pd atom labeled with “1”, as indicated previously by the shortest distance between these fragments and the surface. The CCl_3 fragment is finally adsorbed on the Pd atom (labeled “2”) and the chlorine atom on the next Pd row (Figure 12). After complete dissociation of the first C–Cl bond, three Pd atoms are required for the adsorption of the resulting fragments (see Figure 13 for the case of CCl_4).

It is apparent from Figure 13 that another chlorine atom of the CCl_3 fragment is also interacting with the Pd surface. The fragment does not retain completely a top orientation. This orientation favors consecutive C–Cl bond scission to form a CCl_2 species. This adsorption configuration does not occur for any of the other family members, which may offer an explanation

(31) Chan, C. W.; Gellman, A. J. *Catal. Lett.* **1998**, *53*, 139–143.

(32) Yang, M. X.; Kash, P. W.; Sun, D. H.; Flynn, G. W.; Bent, B. E.; Holbrook, M. T.; Bare, S. R.; Fischer, D. A.; Gland, J. L. *Surf. Sci.* **1997**, *380*, 151–164.

(33) Yang, M. X.; Sarkar, S.; Bent, B. E.; Bare, S. R.; Holbrook, M. T. *Langmuir* **1997**, *13*, 229–242.

for the experimental result that methane is preferentially formed during the hydrodechlorination of CCl_4 .

4. Discussion

4.1. Reaction Steps of $\text{CH}_{4-x}\text{Cl}_x$ ($x = 1-4$) Compounds.

The collected hydrodechlorination kinetic results of $\text{CH}_{4-x}\text{Cl}_x$ ($x = 1-4$) compounds, such as their rates, rate constants, and equilibrium constants, provide insight into possible hydrodechlorination reaction steps. The generalized reaction steps proposed in Scheme 1 were originally derived for the hydrodechlorination of chlorofluorocarbons.^{7,9,10} We will first examine the rate-determining step for hydrodechlorination. In a previous publication,⁷ we found that, for the group of $\text{CF}_3\text{CF}_{4-x}\text{Cl}_x$ ($x = 1-3$) compounds, the relative rate of hydrodechlorination correlated with the bond energy of the first C–Cl bond to break. We proposed that the first C–Cl bond scission is rate-limiting for these compounds. A similar correlation was found for $\text{CH}_{4-x}\text{Cl}_x$ ($x = 1-4$) compounds studied here (Figure 4). The agreement between experimental data and the predicted values in Table 2 is acceptable if one considers that the reactivity of these compounds varies by a factor of 10^4 , while using gas-phase C–Cl bond energy as the only parameter for prediction of the relative turnover rate of each compound. The maximum error is at most a factor of 3, except for CCl_4 in which the error is approximately a factor of 50. Note that the predicted rate for this compound is a factor of 10^4 higher than the reference compound so the relative error compared to reference compound is small. We believe this difference can be explained by deactivation. Unlike the other three compounds, Pd/C catalyst deactivated significantly during the hydrodechlorination of CCl_4 in agreement with previous literature reports.^{34–36} The development of a durable CCl_4 hydrodechlorination catalyst has been attempted,^{34,35} but under the experimental conditions of this study deactivation could not be avoided. The correlation between bond strength and the turnover rate suggests that the first C–Cl bond scission step is once again rate-limiting for hydrodechlorination for each of the chlorinated methane compounds. A Polanyi-type correlation between the apparent activation energy determined by kinetic modeling (Figure 4) and DFT-calculated values of the same parameter and gas-phase C–Cl bond strength of these compounds further supports C–Cl bond scission as the rate-limiting step (Figure 6). It is apparent from Figure 6 that the activation energies determined from the experimental data and DFT calculations are in good agreement with each other.

The finding that the rate limiting step is the same for the families $\text{CH}_{4-x}\text{Cl}_x$ ($x = 1-4$) and $\text{CF}_3\text{CF}_{3-x}\text{Cl}_x$ ($x = 1-3$) suggests that the proposed reaction steps is common for these compounds. Scheme 1 is a general set of reaction steps that apparently can be used to describe the kinetics of hydrodechlorination for other chlorinated compounds. The rate constant for the rate-determining step can be estimated from the strength of the C–Cl bond thus providing an estimate of the overall rate for any compound containing chlorine.

4.2. Comparison between Apparent HCl Reaction Orders of Chlorinated Methane Compounds and Chlorofluorocarbons (CFCs). The measured apparent HCl reaction orders for the chlorinated methane compounds were less negative than the HCl orders for CF_3CFHCl (Table 1). The apparent reaction order is defined as the coefficient “c” in the power rate law $r = k'[\text{CFC}]^a[\text{H}_2]^b[\text{HCl}]^c$. However, we have shown that the rate expression

that best describes this reaction is $r = k'[\text{CFC}]/(1 + K'[\text{HCl}]/[\text{H}_2]^{1/2})$ where k' and K' have been defined in eq 9. This expression can be simplified into a power rate law if the magnitude of $K'[\text{HCl}]/[\text{H}_2]^{1/2}$ in the denominator is large compared to 1. When this assumption is met, the rate expression can be described as a power-rate law and the HCl reaction order will be -1 . The value of the exponent on the HCl concentration depends on the magnitude of the term $K'[\text{HCl}]/[\text{H}_2]^{1/2}$ relative to unity. The apparent reaction order in HCl can vary between -1 and 0 according to eq 9. The magnitudes of K' (Figure 5) for CF_3CFHCl were higher than those for $\text{CH}_{4-x}\text{Cl}_x$ ($x = 1-4$) compounds under the same reaction conditions. The values for K' for the different chlorinated methane compounds are different, although eq 6 predicts that K' should be independent of the chlorinated hydrocarbon. The explanation for the discrepancy is probably due to the fact that the experiments were performed over a range of temperatures ($\Delta T = 165$ °C) which will change the chlorine surface coverage (the most abundant surface intermediate) significantly due to changes in K_{CFC} with temperature. The rate and equilibrium constants are a function of temperature which also controls surface coverage, and the changes we observe in the values of these constants are an indication of these interactions.

The apparent HCl order approaches -1 as the temperature decreases for a single component (data not shown). The constant K' is related to the equilibrium constant of reaction 6. Figure 5 shows the heat of reaction is negative, and correspondingly, the value of K' decreases with increasing temperature. The rate expression (eq 9) can be approximated by a power law rate law as $K'[\text{HCl}]/[\text{H}_2]^{0.5} \gg 1$, which will occur as the measured apparent HCl reaction order approaches -1 .

4.3. Reaction Orders for CHCl_3 and CCl_4 Are Lower than Unity. The reaction orders of CH_3Cl and CH_2Cl_2 were close to unity, similar to the value for CF_3CFHCl . The reaction orders for CHCl_3 and CCl_4 are lower than unity; we believe this is due to the condensation of the chlorinated compounds in the pores of the carbon support. In a previous publication,⁷ we found the reaction order in CF_3CFCl_2 was less than unity, and the adsorption isotherms of CF_3CFCl_2 on the high-surface area carbon demonstrated that the micropores of the carbon are filled with condensed CF_3CFCl_2 (the boiling point of CF_3CFCl_2 is 3.6 °C) even at an adsorption temperature of 100 °C. If a reactant fills the support pore, it will not respond to changes in its gas-phase concentration, and the reaction order will be equal to or less than zero (effectively, the surface concentration C_s will be greater than the bulk concentration (partial pressure)). The boiling points of CHCl_3 and CCl_4 (61 and 77 °C, respectively) are close to the HDCl reaction temperature (114 and 61 °C, respectively). It is believed that partial condensation of reactants resulted in a lower reaction order in the chlorinated organic compound. We were unable to conduct the reaction of CHCl_3 and CCl_4 at higher temperatures (to eliminate or minimize pore condensation) because the reactant conversion would be close to 100% .

4.4. Reaction Selectivity in the Presence of Deuterium. The products of hydrodechlorination of the series of chlorinated methane compounds vary from only one in the case of CH_3Cl up to four for CCl_4 (chlorine is removed one at a time, regardless of the number of chlorines in the molecule), although DFT calculations of CCl_4 adsorption on Pd(110) suggest that the CCl_3 is quickly converted to CH_2 due the strong interaction of one of the Cl atoms in the adsorbed CCl_3 fragment (see section 4.6). Product selectivity was independent of conversion (section 3.2), implying that once a hydrodechlorination product reaches the gas phase, it does not readsorb and react. This is due to the fact that the hydrodechlorination reaction products are much less

(34) Zhang, Z. *Treatment to improve the durability and selectivity of supported noble metal hydrodechlorination catalysts*; U.S. Patent 5962366, 1999.

(35) Zhang, Z. C.; Beard, B. *Appl. Catal., A* **1998**, *174*, 33–39.

(36) Lokteva, E. S.; Simagina, V. I.; Golubina, E. V.; Stoyanova, I. V.; Lunin, V. V. *Kinet. Catal.* **2000**, *41*, 776–781.

reactive than the reactant (see Table 1). For example, the product CH_3Cl is 100 times less reactive than CH_2Cl_2 .

During the hydrodechlorination of CH_3Cl and CH_2Cl_2 , the products detected formed through C–Cl bond scission as well as C–H bond scission. For example, in the case of CH_2Cl_2 , both CHD_3 (7.5% selectivity) and perdeuterated methane (13.6% selectivity) were observed in the gas phase. The product distribution demonstrates that the pool of surface intermediates is diverse because products which have undergone H/D exchange with incomplete hydrodechlorination (CD_3Cl and CHD_2Cl) are observed in the gas-phase during CH_2Cl_2 HDCl. A similar observation is noted in the distribution of deuterium in the gas-phase products during the HDCl of CHCl_3 in D_2 (Figure 7). During the hydrodechlorination of CCl_4 and CHCl_3 , C_2 – C_5 hydrocarbon species produced by C–C bond formation accompanied the C_1 hydrodechlorination products. Previous hydrodechlorination studies of CCl_4 reported the formation of longer chain hydrocarbons which increased at higher temperature.^{36,37}

4.5. Reaction Steps beyond the Rate-Determining Step.

The prediction of product distribution can only be achieved with a more detailed set of reaction steps with the inclusion of the reaction steps (i.e., C–H bond scission) beyond the rate-determining step. Campbell and Kembal¹¹ reported during D_2 exchange of $\text{CH}_3\text{CH}_2\text{Cl}$, the doubly deuterated product CH_3CHD_2 was the most abundant. They concluded that during the hydrodechlorination of $\text{CH}_3\text{CH}_2\text{Cl}$, both the C–Cl bond and C–H bond in the same carbon broke. During D_2 exchange experiments of CF_3 – CHFCl , 98% of the product was CF_3 – CFHD .¹⁰ The deuterated product distribution for CH_2Cl_2 and CHCl_3 in Figure 7 demonstrated no significant C–H bond scission accompanies the first C–Cl bond scission, similar to previous results for CF_3CHFCl .⁸ In the case of CH_2Cl_2 HDCl, the selectivity to CD_3Cl and CHD_2Cl is only 2.2%, similar to the 98% selectivity observed for CF_3 – CFHCl . C–H bond scission occurs more readily during scission of the second and third C–Cl bond in CH_2Cl_2 and CHCl_3 (Figure 7) than during the scission of the first C–Cl bond. The rate of exchange of hydrogen to deuterium in the adsorbed molecule increases as the degree of dechlorination increases. Thus, for the scission of the second and third C–Cl bond in CH_2Cl_2 and CHCl_3 (Figure 7), C–H bond scission of the adsorbed fragments becomes more pronounced, suggesting that the surface chemistry becomes more complex and the number of distinct reactive intermediates increases.

4.6. Correlation between Experimental Results and Periodic DFT Calculations. The activation energies determined from kinetic modeling and DFT calculations are quite similar (comparison

between Figure 4 and Table 3). All of the DFT calculations were calculated at a coverage of 1/9 ML (Figure 10). Although we predict under reaction conditions the coverage of Cl would be considerably higher, the values are in good agreement, suggesting that a pair of nearest neighbor Pd atoms are required to break the first C–Cl bond for the less-chlorinated methane compounds (i.e., CH_3Cl and CH_2Cl_2 (Figure 10)), while CCl_4 may require a larger ensemble of atoms (Figure 13). In the case of CCl_4 , the dissociated chlorine is actually more stable on an atom of an adjacent row rather than an adjacent atom in the same row where the CCl_3 fragment is adsorbed. In this example, three Pd atoms are required to stabilize the CCl_3 fragment and Cl on the surface. It does not appear that the activation energy determined from kinetic modeling is sensitive to these possible differences in site requirements for the dissociation of the first C–Cl bond across the family of chlorinated methane compounds.

5. Conclusions

The hydrodechlorination reaction kinetics of a series of chlorinated methane compounds, $\text{CH}_{4-x}\text{Cl}_x$ ($x = 1-4$), were examined and compared with previously reported kinetics for CFC compounds. It is found that the rate of hydrodechlorination of these chlorinated hydrocarbons depended on the strength of the first C–Cl bond broken. A Polanyi-type relationship exists between the activation energy of the scission of the first C–Cl bond and the C–Cl bond energy. These results support the scission of the first C–Cl bond as the rate-determining step in hydrodechlorination. The reaction kinetics of these compounds can be described by a Langmuir–Hinshelwood type rate expression $r = k'[\text{R-Cl}]/(1 + K'[\text{HCl}]/[\text{H}_2]^{0.5})$, where k' and K' represent lumped kinetic and thermodynamic constants dependent only on temperature. The reaction steps are similar to a previously proposed set of reaction steps, indicating that these reaction steps might be generally valid for describing the reaction kinetics of Pd-catalyzed hydrodechlorination. The reaction steps beyond C–Cl bond scission step were probed using D_2 isotopic tracing techniques. No significant C–H bond scission accompanied scission of the first C–Cl bond, similar to results obtained with CF_3 – CFHCl . The number of chlorine atoms in the members of $\text{CH}_x\text{Cl}_{4-x}$ family plays an important role in the energetic of dissociation of the first C–Cl bond as demonstrated by DFT calculations. The number of chlorine atoms not only modifies the geometry of the transition state of the dissociation reaction but also influences the stability of the resulting adsorbed fragments of the dissociated $\text{CH}_{4-x}\text{Cl}_x$ species. DFT-calculated activation energies and activation energies determined from kinetic modeling for C–Cl bond breaking are in good agreement with each other, and they scale linearly with gas-phase C–Cl bond energy of the chlorinated methane compounds.

(37) Lokteva, E. S.; Lunin, V. V.; Golubina, E. V.; Simagina, V. I.; Egorova, M.; Stoyanova, I. V. *Stud. Surf. Sci. Catal.* **2000**, *130C*, 1997–2002.